Supplementary Material for: "Predictor/corrector methods for efficient and stable propagation of the time-dependent Kohn-Sham equation"

Ying Zhu and John M. Herbert*
Department of Chemistry and Biochemistry, The Ohio State University, Columbus, Ohio 43210 USA
(Dated: January 13, 2018)

A. Instability of the LFLP-PC3 algorithm

We find that the LFLP-PC3 algorithm, in which the initial predictor matrix $\mathbf{F}^{\mathrm{p}}_{N+1/2}$ is always averaged with the current corrector matrix $\mathbf{F}^{\mathrm{c}}_{N+1/2}$ to estimate the half-step Fock matrix, is unstable even when Δt is small. This is similar to known instabilities in the case of the ordinary differential equation, where the use of the average of the initial predicted value and the final corrected value as the starting point for the next iteration can be unstable,[1] though in our experience no such instability exists in the case of the EP-PC propagator. Figure S1 shows the that the induced dipole moment diverges when the LFLP-PC3 algorithm is used, even for a time step as small as 0.2 a.u. The simulation is for a single H_2O molecule, subject to a δ-function pulse of 10^{-5} a.u. during the first time step; the plot in Fig. S1(a) is a stable reference calculation obtained using the LFLP-PC1 algorithm. In the latter case, the induced dipole moment undergoes small but stable fluctuations as large as $\sim 4 \times 10^{-5}$ D. Even with $\Delta t = 0.2$ a.u., however, the LFLP-PC3 algorithm rapidly leads to fluctuations as large as several a.u. in magnitude (1 a.u. = 2.542 D), which is obviously unphysical and indicates numerical instability in the electron dynamics.

B. Divergence of the MMUT algorithm for large time steps

Figure S2 plots energy fluctuations $|\Delta E| = |E_N - E_{N-1}|$ for TDKS simulations of H_2O subject to impulsive fields ranging in magnitude from 10^{-3} a.u. and 10^{-1} a.u. Data are presented for the MMUT and EP-PC1 propagator algorithms, and these data complement those presented in Figs. 4 and 5 in the main text. The MMUT propagator is clearly unstable for $\Delta \geq 0.2$ a.u., for both the PBE and LRC-ωPBEh functionals, and even $\Delta t = 0.1$ a.u. is problematic for LRC-ωPBEh. This is consistent with our general conclusion that the use of Hartree-Fock exchange leads to faster time-scale fluctuations in the Fock and density matrices and thus necessitates somewhat smaller time steps and/or tighter convergence thresholds. Instability in the MMUT simulations for large time steps is also observed in the form of a divergent dipole moment, the fluctuations in which are plotted in Fig. S3. For the EP-PC1 simulations, the dipole moment is stable with fluctuations in the induced dipole moment $\sim 2 \times 10^{-3}$ a.u. (Fig. S4). The total (signed) energy change for the EP-PC1 simulations, starting from the ground-state energy, is plotted in Fig. S5 for various time steps and a pulse amplitude of 0.02 a.u. The frequency of the pulse corresponds to about 12 eV in energy units, which excites the bright state of H_2O. This resonant excitation causes the system to gain energy while the pulse is turned on, and induces resonant oscillations in the electron density. Finally, absorption cross sections for the TDKS simulations in Fig. S2 are plotted in Fig. S6. The latter data complement those presented in Fig. 6 of the main text.

C. Role of the threshold ξ

Components of the induced dipole moment $\delta\boldsymbol{\mu}$, for H_2O at the PBE/6-31G(d) level, are plotted in Fig. S7 and analogous results at the LRC-ωPBEh/6-31G(d) level are shown in Fig. S8, using the EP-PC1 algorithm in each case. The external field is a δ-function kick at $t = 0$ in the $(1, 1, 1)$ with an amplitude of 10^{-5} a.u. in each case, and the various plots show the effect of various choices of the threshold ξ. The primary role of this threshold is different for the two different functionals. For PBE, reducing ξ serves mainly to prevent the appearance of noise in the long-time propagation of the dipole moment; for sufficiently small values of ξ, fluctuations in $\|\delta\boldsymbol{\mu}\|$ do not increase in magnitude over time. In the case of the non-local LRC-ωPBEh functional, a too-loose value of ξ serves to dampen the fluctuations in $\delta\boldsymbol{\mu}$ too quickly, leading to errors in $S(\omega)$.

Figure 8 in the main text shows TDKS absorption spectra, computed with the EP-PC3 algorithm at the PBE/6-31G(d) level, for various values of ξ. Analogous spectra computed using other PC propagators are provided in

* herbert@chemistry.ohio-state.edu

Figs. S9–S12. As in Fig. 8, these simulations correspond to a single H_2O and a total propagation time of 5,000 a.u., with $\Delta t = 0.5$ a.u.

D. Convergence of spectra with respect to Δt

Finally, we consider the convergence of the absorption spectrum for adenine with respect to the choice of time step. Results shown in Figs. S13–S14 using time steps as short as $\Delta t = 0.02$ a.u. show that there is virtually no difference as compared to spectra computed using $\Delta t = 0.2$ a.u., up to at least 50 eV, which justifies the use of the latter as reference spectra in the main document. Convergence of the spectrum using various propagators is shown in Figs. S15–S18, which complement EP-PC3 results in Fig. 9.

---

[1] R. W. Hamming, *Numerical Methods for Scientists and Engineers*, Dover Publications, Inc., New York, NY, USA, 2nd edition, 1986.

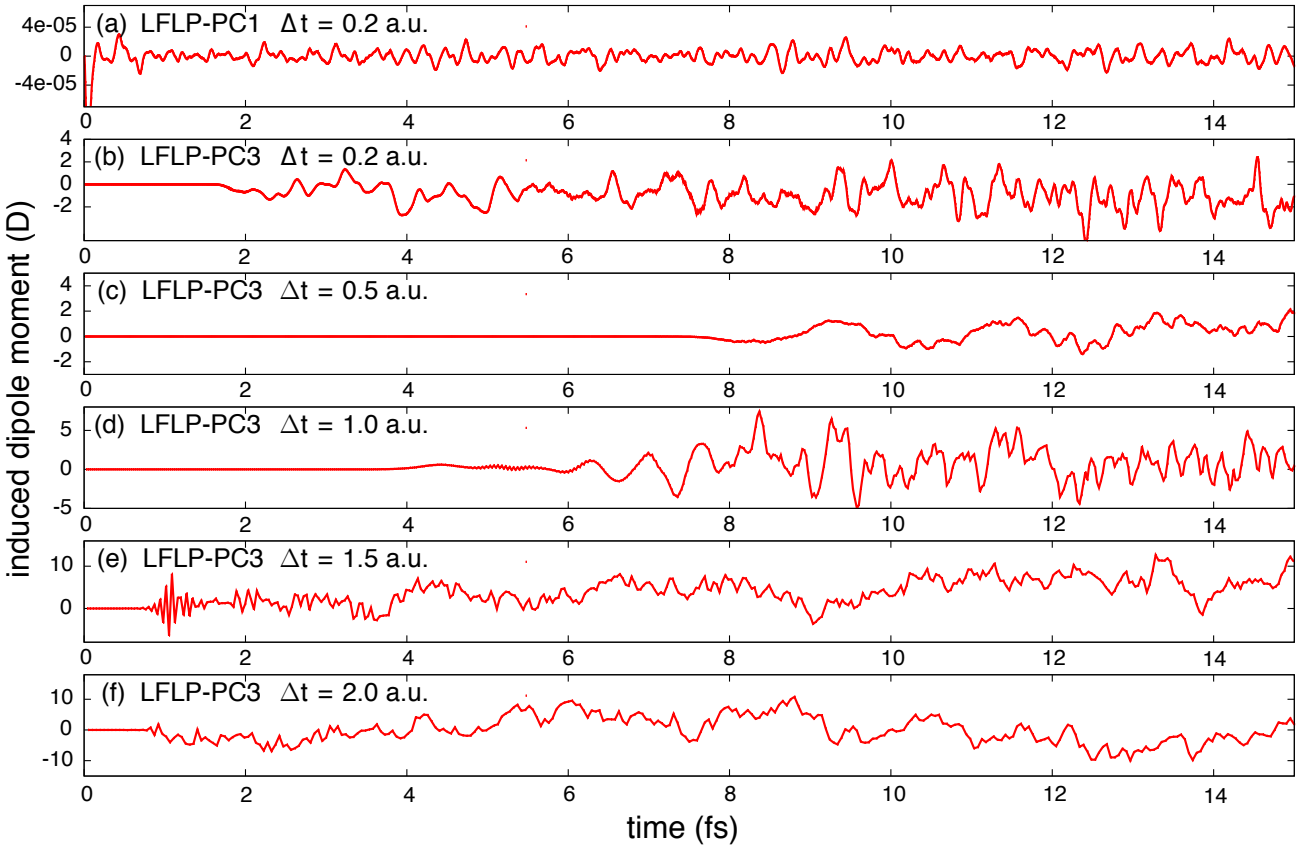

FIG. S1: Induced dipole moment in the z direction for H_2O subject to a weak δ-function perturbation at $t = 0$. The LFLP-PC1 result in (a) provides a stable reference. In (b)–(f), the LFLP-PC3 algorithm is used with various time steps. Even for $\Delta t = 0.2$ a.u., in (b), fluctuations in the dipole moment are unstable. Note the vastly different vertical scale in panel (a) as compared to the other panels.

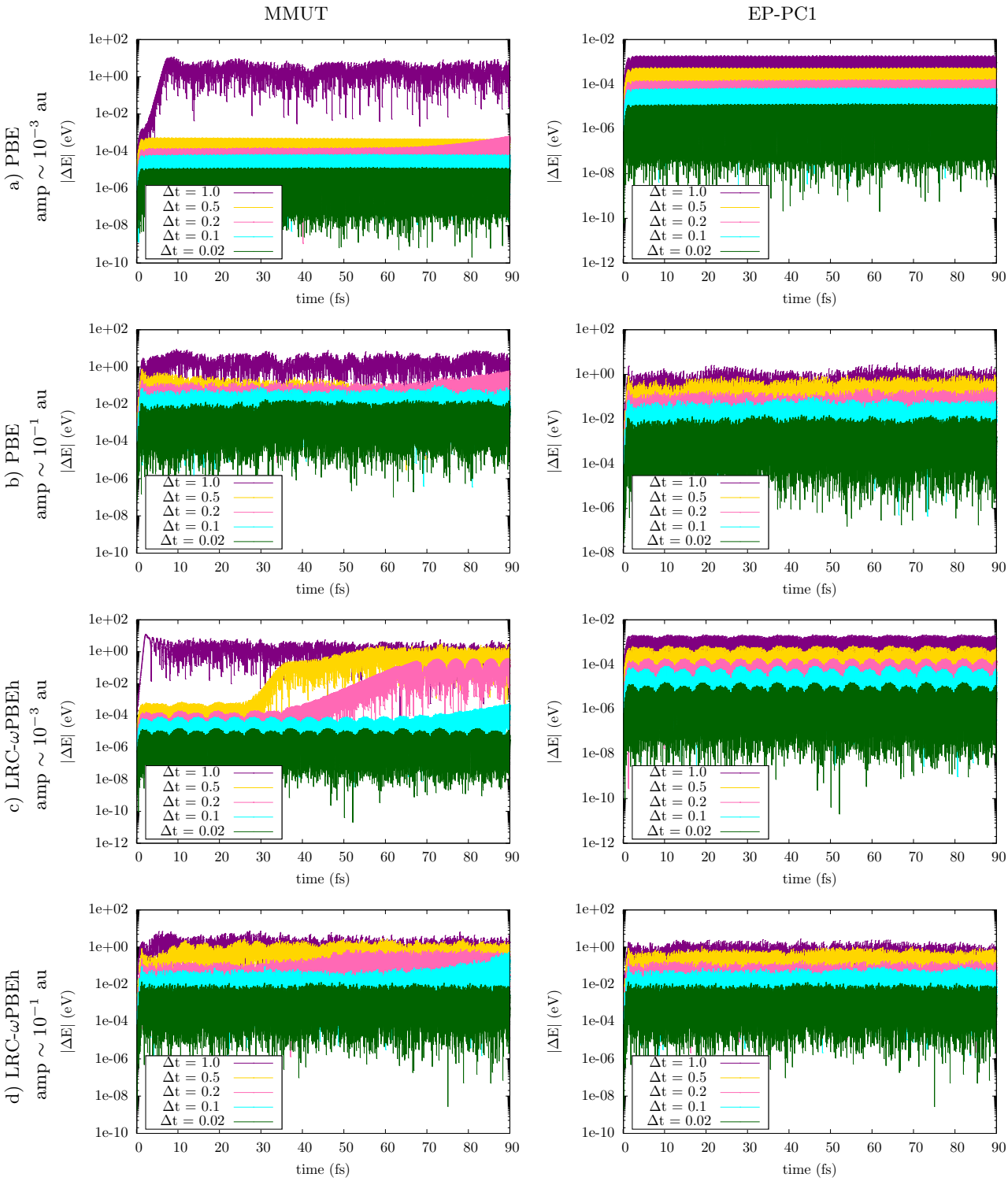

FIG. S2: Fluctuations in the total energy for TDKS simulations of H_2O with two different propagators and various time steps, plotted on a logarithmic scale. Panels on the left use the MMUT propagator algorithm whereas those on the right were obtained using EP-PC1. The exchange-correlation functional and pulse amplitude are indicated along the vertical axis.

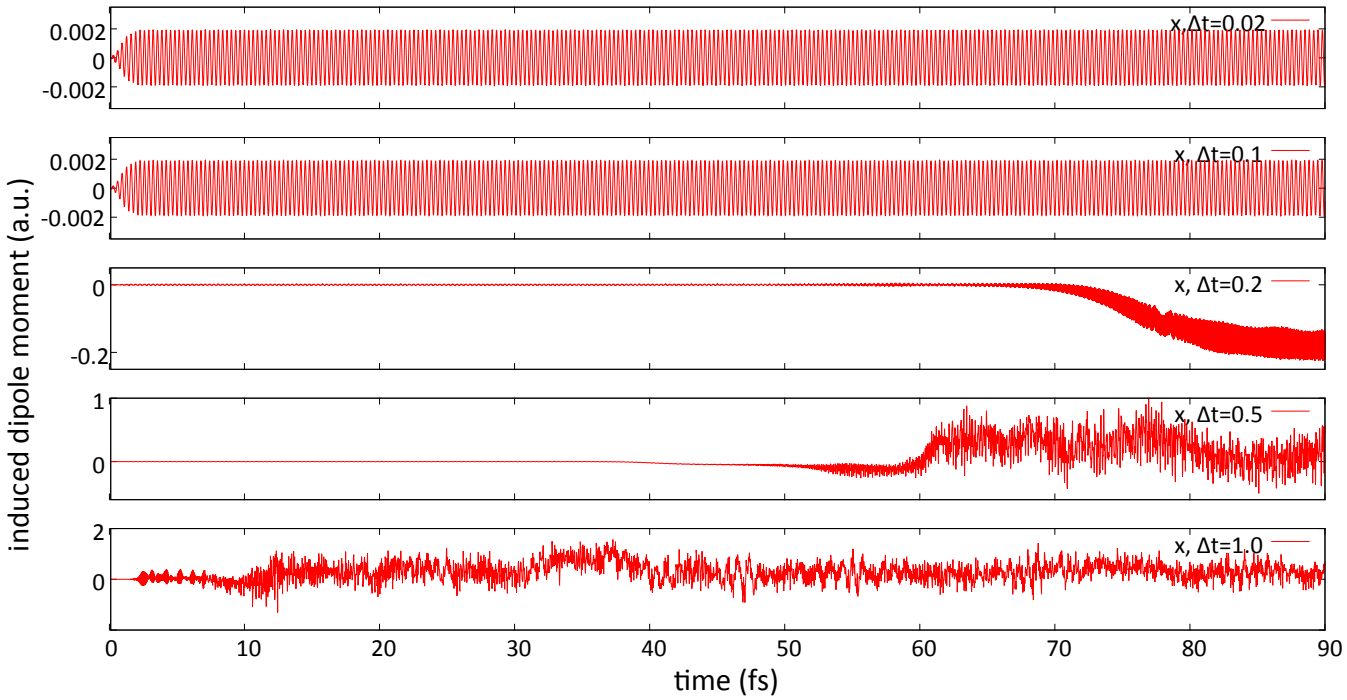

FIG. S3: Induced dipole moment of H_2O in the x direction, computed at the LRC-ωPBEh/6-31G(d) following an impulse whose amplitude is 2×10^{-4} a.u. The TDKS dynamics were propagated using the MMUT algorithm, for which the resonant response in the dipole moment diverges for $\Delta t > 0.1$ a.u. Note the vastly different scale for $\Delta t > 0.1$ a.u. as compared to $\Delta t = 0.02$ a.u.

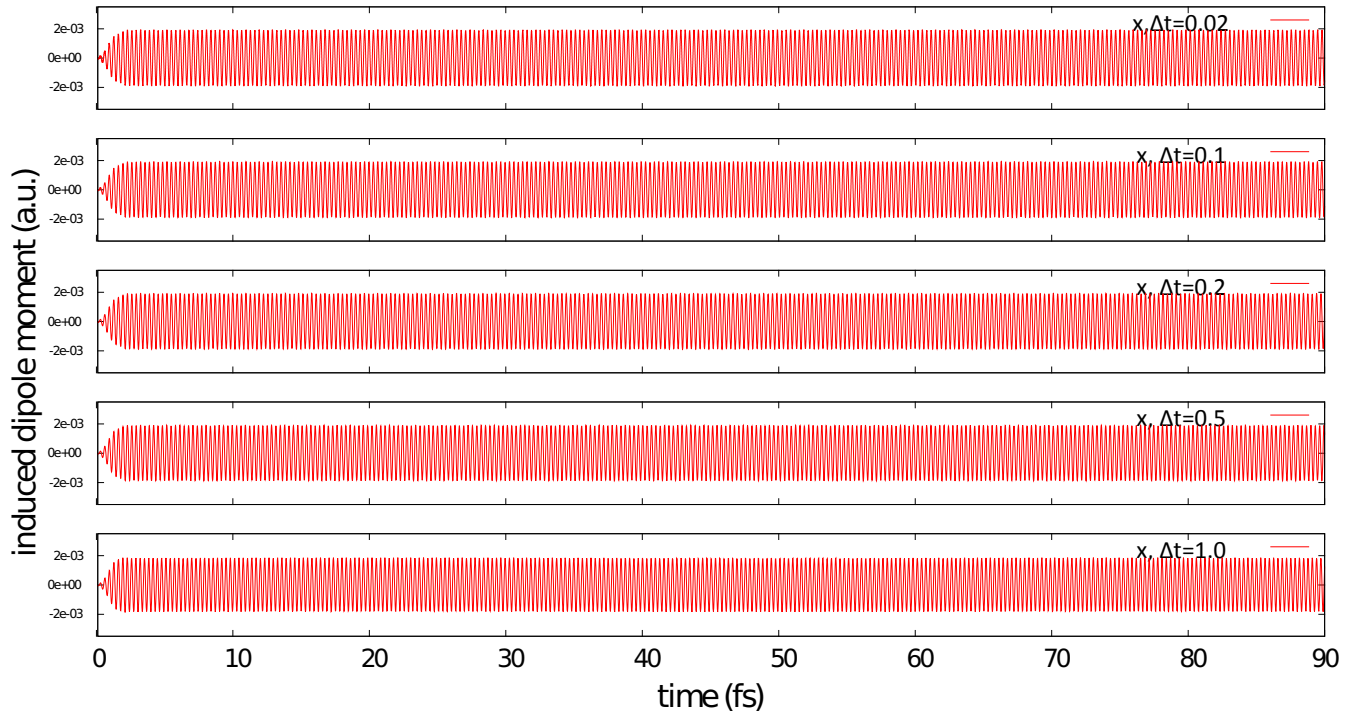

FIG. S4: Induced dipole moment of H_2O in the x direction, computed at the LRC-ωPBEh/6-31G(d) following an impulse whose amplitude is 2×10^{-4} a.u. The TDKS dynamics were propagated using the EP-PC1 algorithm, which affords stable dynamics for all values of Δt examined here.

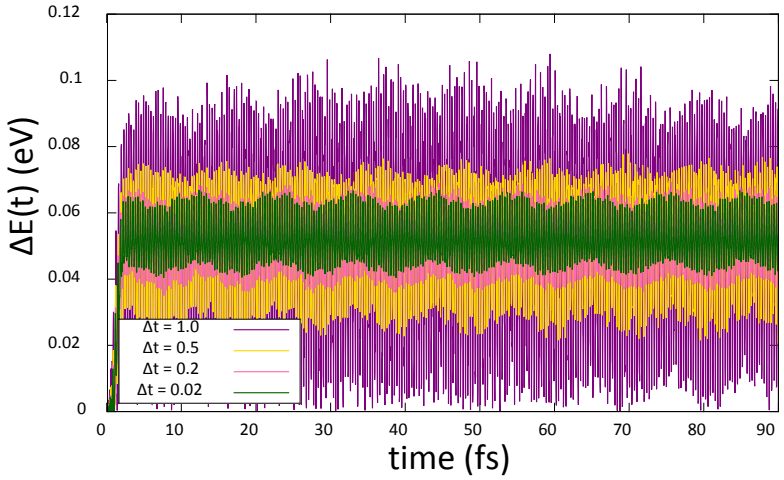

FIG. S5: Absolute energy change $\Delta E = E(t) - E(0)$ for EP-PC1 simulations at the PBE/6-31G(d) level, following an electric field pulse whose amplitude is 0.02 a.u. The pulse causes the total energy to increase by about 0.5 eV, following which the total energy fluctuates around the new value. Larger time steps lead to larger fluctuations in the total energy as a result of numerical error.

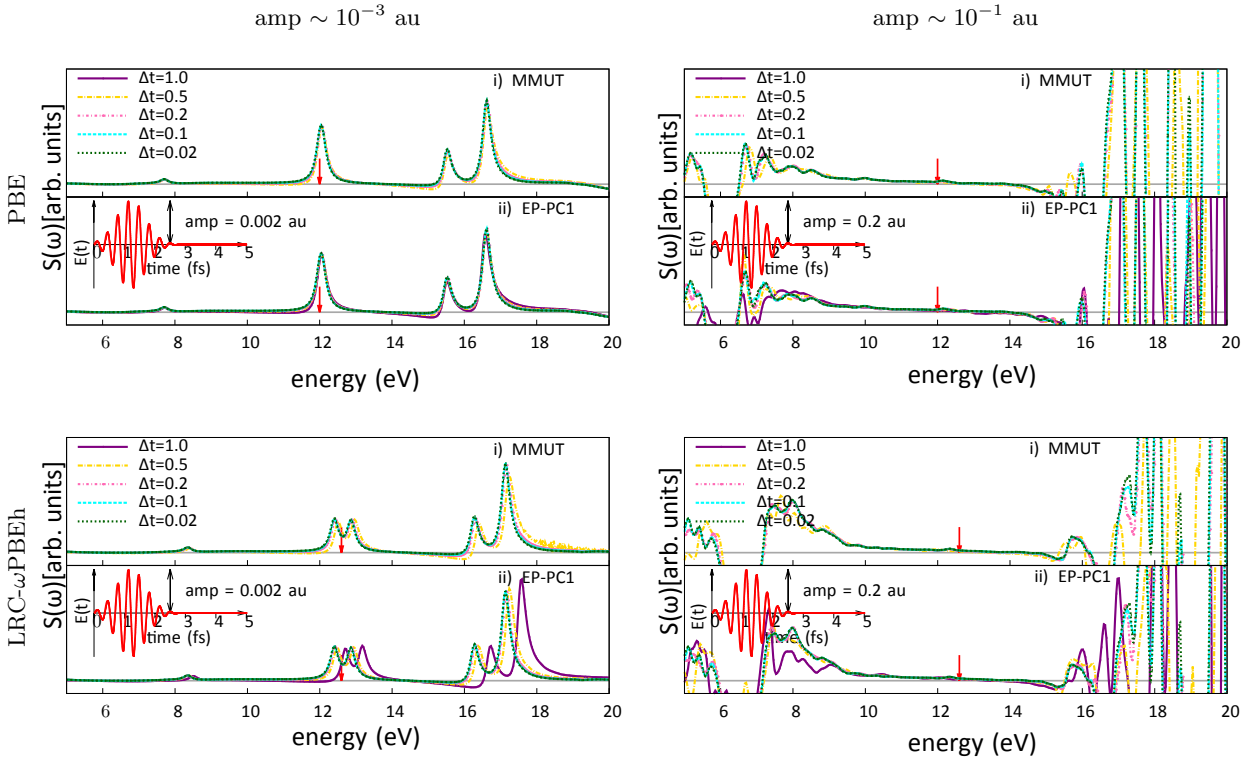

FIG. S6: Absorption cross section $S(\omega)$ for TDKS simulations of H_2O using either the MMUT or EP-PC1 propagator with various time steps; these are the same simulations whose energy fluctuations are plotted in Fig. S2. The gray horizontal line in the background indicates where $S(\omega) \equiv 0$. The time-dependent external field is plotted in red and the red arrow around 12 eV shows where the field frequency shows up in energy units. The field amplitude is 0.001 a.u. for the panels on the left and 0.1 a.u. for the panels on the right. The two panels on top use the PBE/6-31G(d) level of theory while on the bottom it is LRC-ωPBEh/6-31G(d).

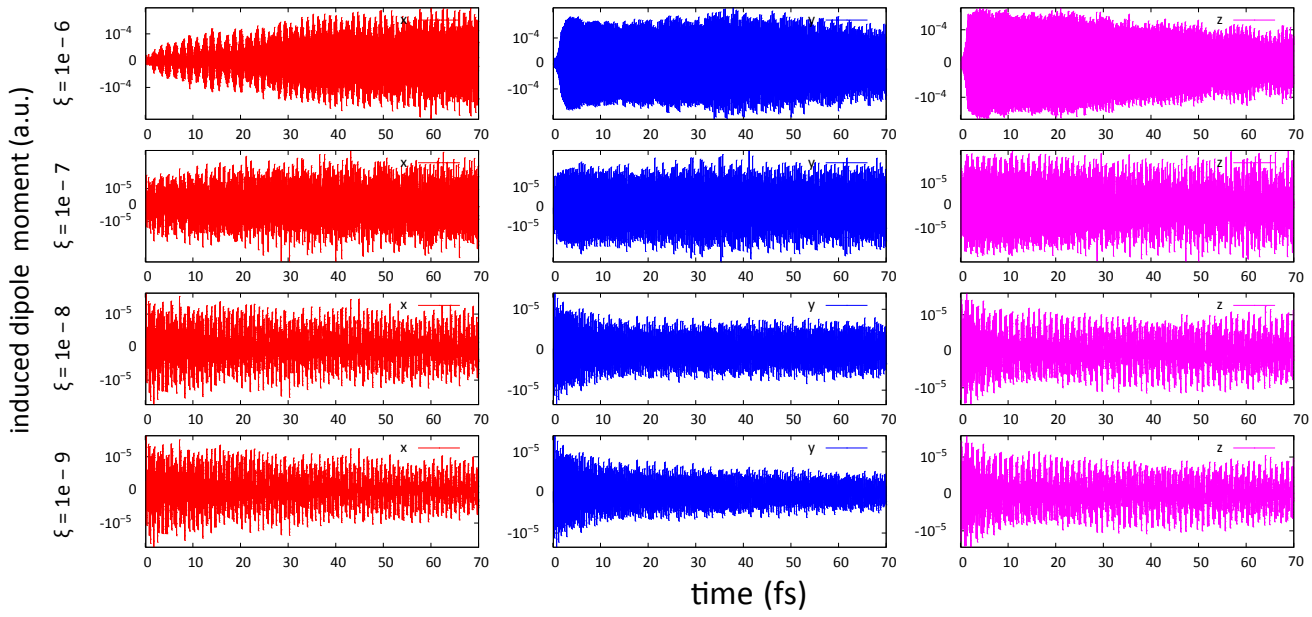

FIG. S7: Components of the induced dipole moment (in a.u.) for H_2O at the PBE/6-31G(d) level using the EP-PC1 propagator with thresholds ξ ranging from 10^{-6}–10^{-9}. The external field is a δ-function pulse at $t = 0$ with an amplitude of 10^{-5} a.u. The red, blue, and magenta plots are the x, y, and z components of $\delta\boldsymbol{\mu}$, respectively.

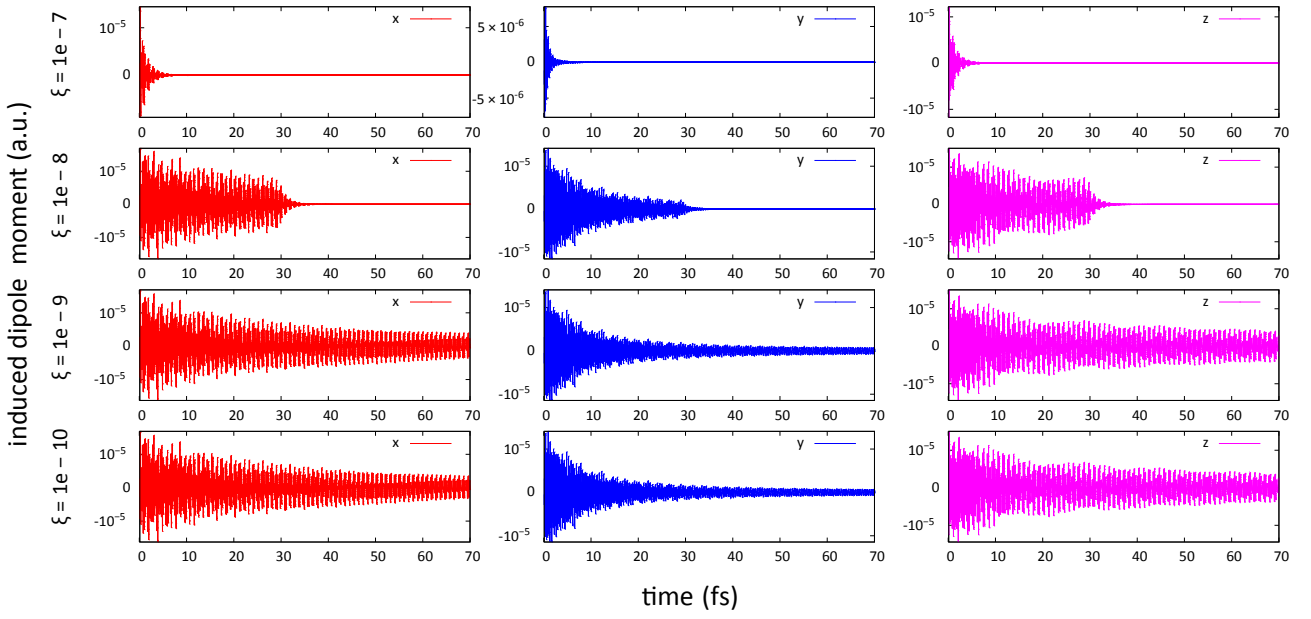

FIG. S8: Components of the induced dipole moment (in a.u.) for H_2O at the LRC-ωPBEh/6-31G(d) level using the EP-PC1 propagator with thresholds ξ ranging from 10^{-7}–10^{-10}. The external field is a δ-function pulse at $t = 0$ with an amplitude of 10^{-5} a.u. The red, blue, and magenta plots are the x, y, and z components of $\delta\boldsymbol{\mu}$, respectively.

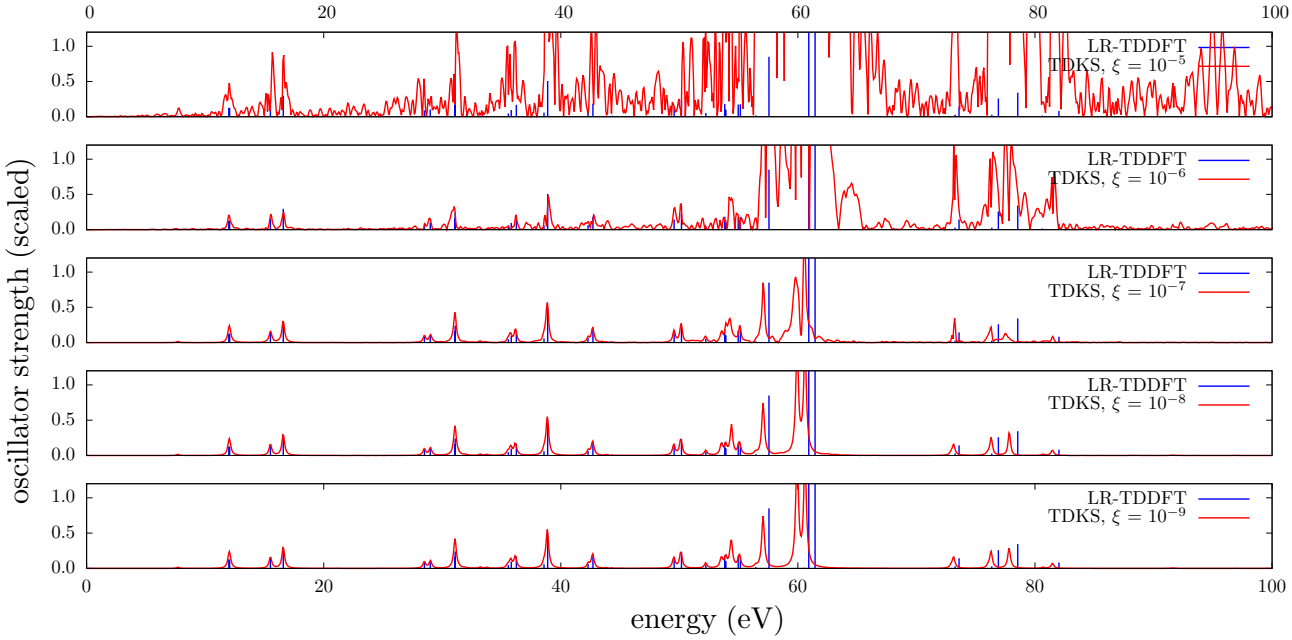

FIG. S9: TDKS spectra of H_2O computed using the LFLP-PC1 algorithm (red curves) with various values of ξ. For reference, as LR-TDDFT stick spectrum is shown in blue. TDKS simulations were propagated for $T = 5,000$ a.u. using $\Delta t = 0.5$ a.u., and all TDKS spectra were scaled by a common, empirical factor to best match the LR-TDDFT intensities.

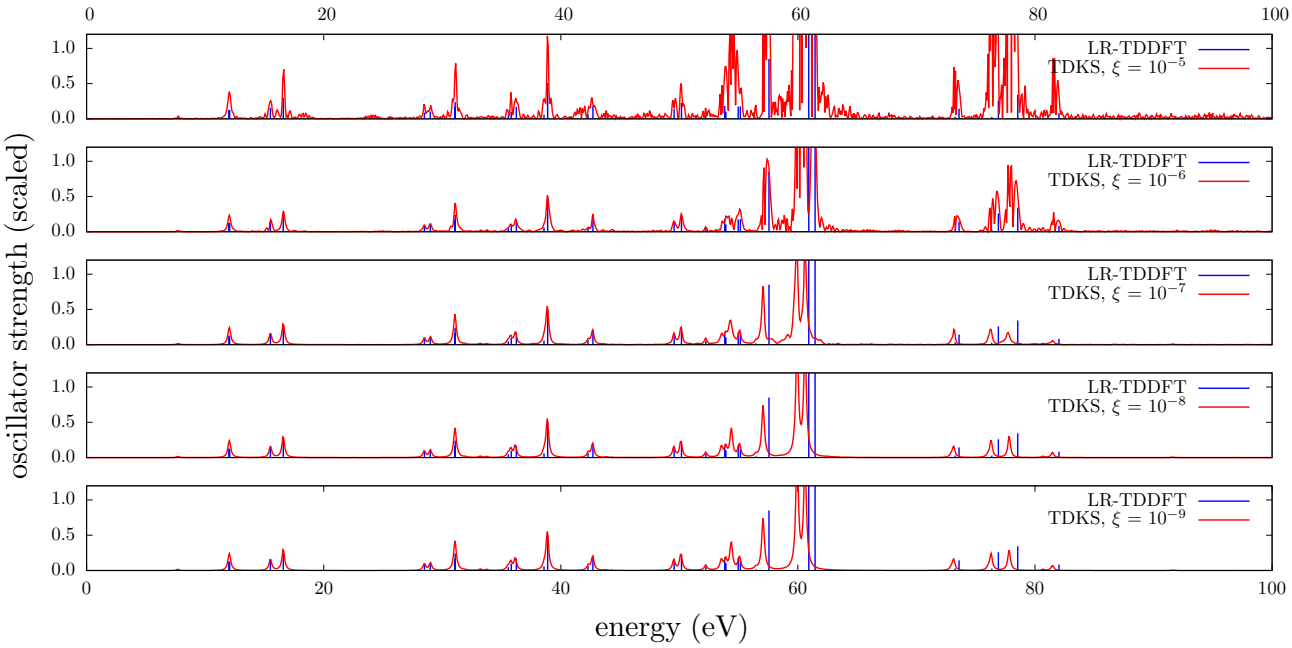

FIG. S10: TDKS spectra of H_2O computed using the LFLP-PC2 algorithm (red curves) with various values of ξ. For reference, as LR-TDDFT stick spectrum is shown in blue. TDKS simulations were propagated for $T = 5,000$ a.u. using $\Delta t = 0.5$ a.u., and all TDKS spectra were scaled by a common, empirical factor to best match the LR-TDDFT intensities.

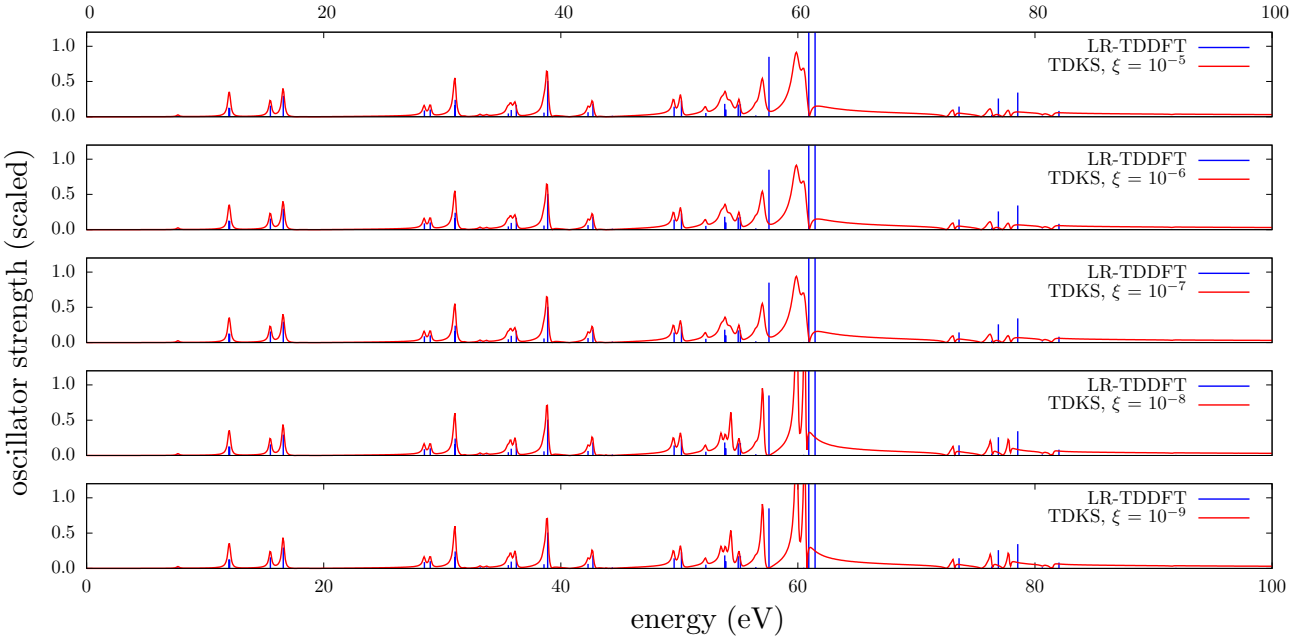

FIG. S11: TDKS spectra of H_2O computed using the EP-PC1 algorithm (red curves) with various values of ξ. For reference, as LR-TDDFT stick spectrum is shown in blue. TDKS simulations were propagated for $T = 5,000$ a.u. using $\Delta t = 0.5$ a.u., and all TDKS spectra were scaled by a common, empirical factor to best match the LR-TDDFT intensities.

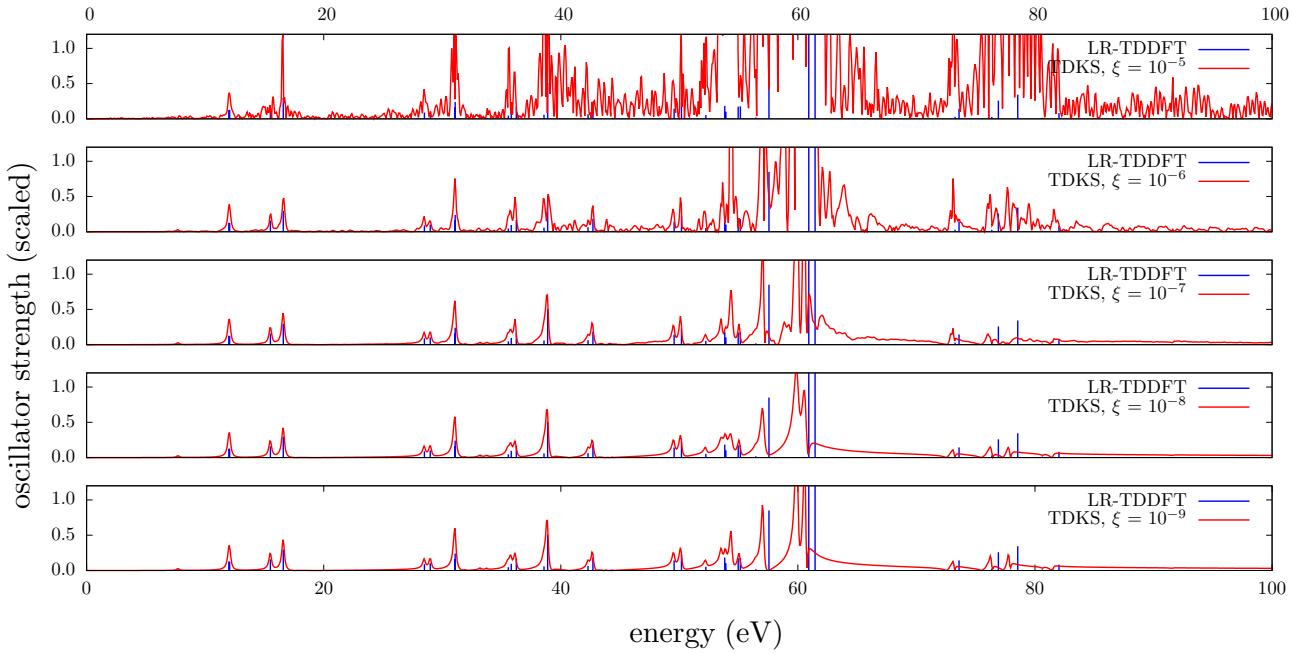

FIG. S12: TDKS spectra of H_2O computed using the EP-PC2 algorithm (red curves) with various values of ξ. For reference, as LR-TDDFT stick spectrum is shown in blue. TDKS simulations were propagated for $T = 5,000$ a.u. using $\Delta t = 0.5$ a.u., and all TDKS spectra were scaled by a common, empirical factor to best match the LR-TDDFT intensities.

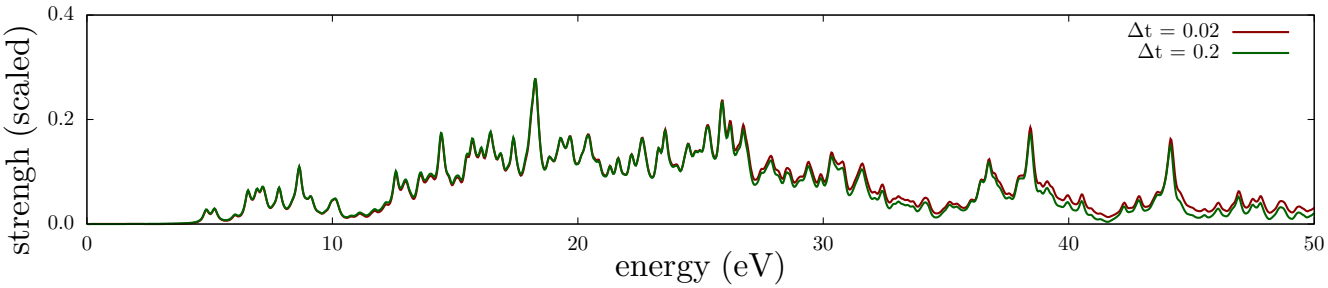

FIG. S13: TDKS spectra of adenine at the PBE/6-31G(d) level computed with the EP-PC1 propagator and several different time steps. The total simulation time is the same in either case, 5,000 a.u. (≈ 120 fs).

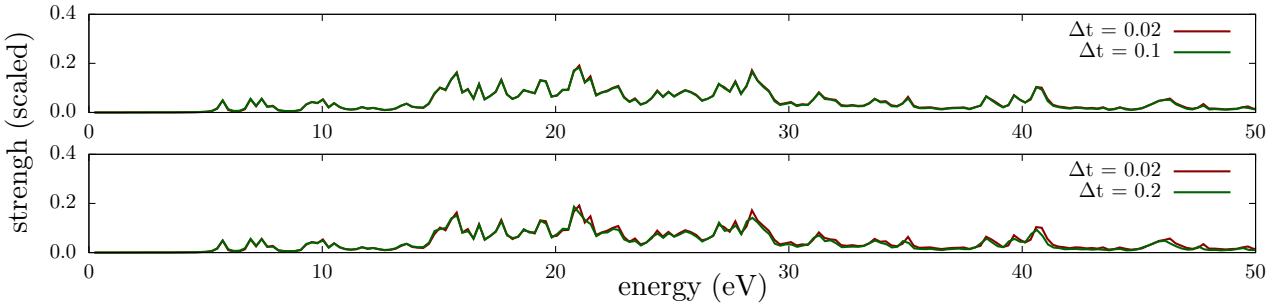

FIG. S14: TDKS spectra of adenine at the LRC-ωPBEh/6-31G(d) level computed with the EP-PC3 propagator and several different time steps. The total simulation time is the same in either case, 716 a.u. (≈ 17.3 fs).

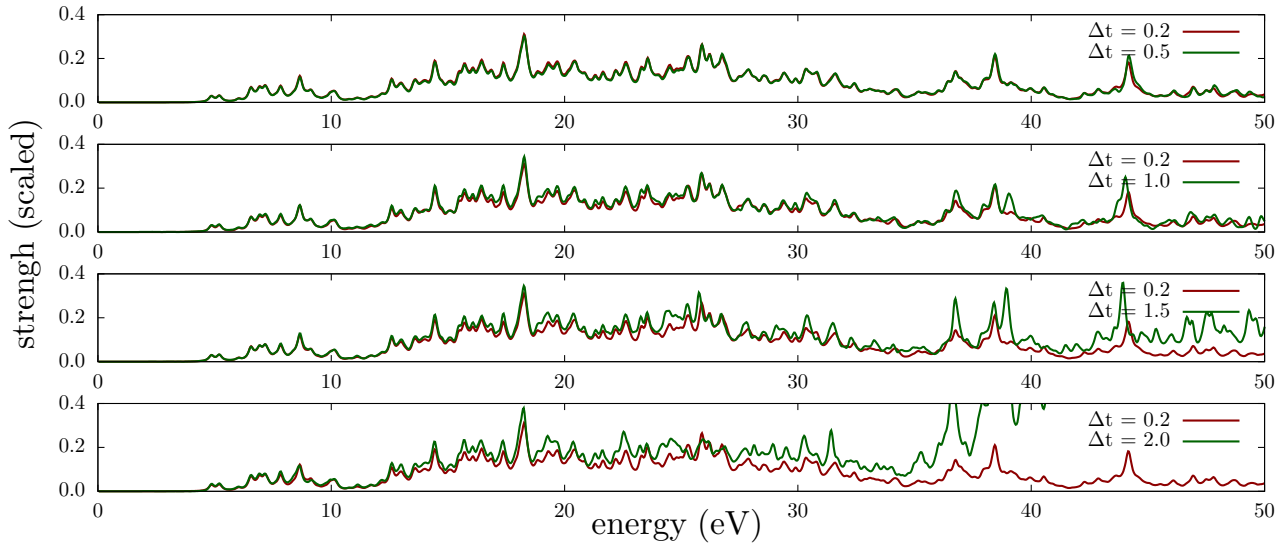

FIG. S15: TDKS spectrum of adenine computed using the LFLP-PC1 algorithm for various values of Δt. The reference spectrum, computed using $\Delta t = 0.2$ a.u., is shown in red.

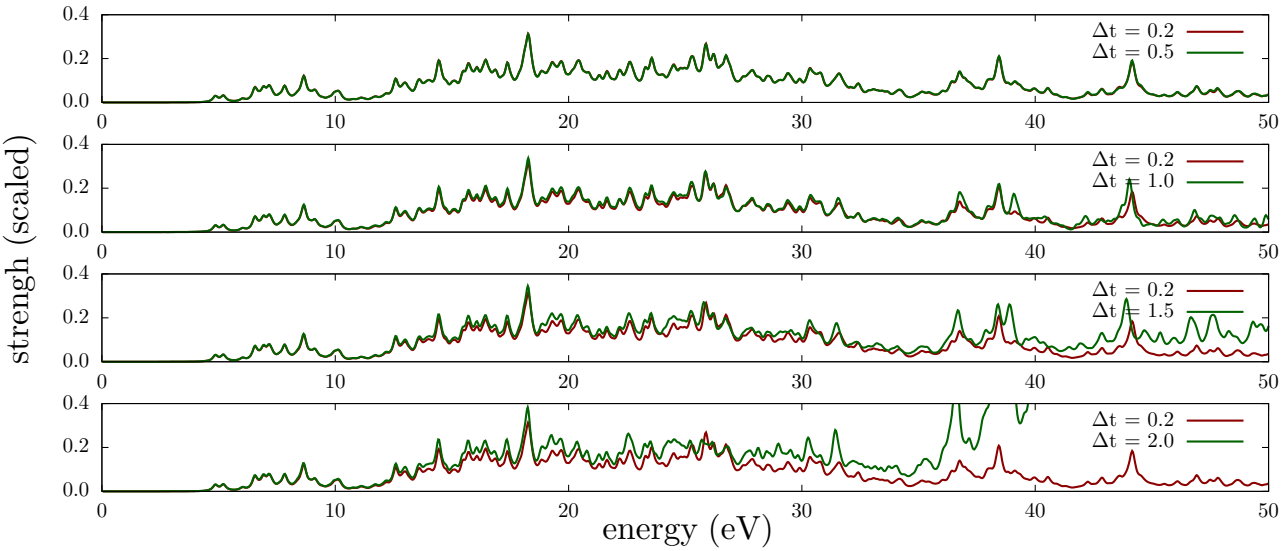

FIG. S16: TDKS spectrum of adenine computed using the LFLP-PC2 algorithm for various values of Δt. The reference spectrum, computed using $\Delta t = 0.2$ a.u., is shown in red.

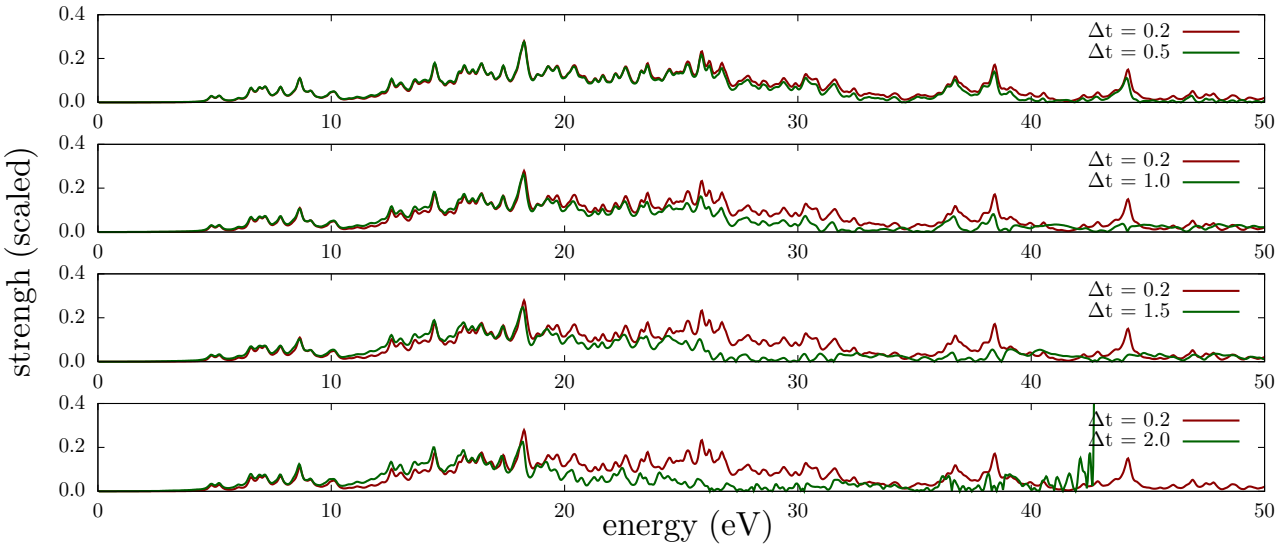

FIG. S17: TDKS spectrum of adenine computed using the EP-PC1 algorithm for various values of Δt. The reference spectrum, computed using $\Delta t = 0.2$ a.u., is shown in red.

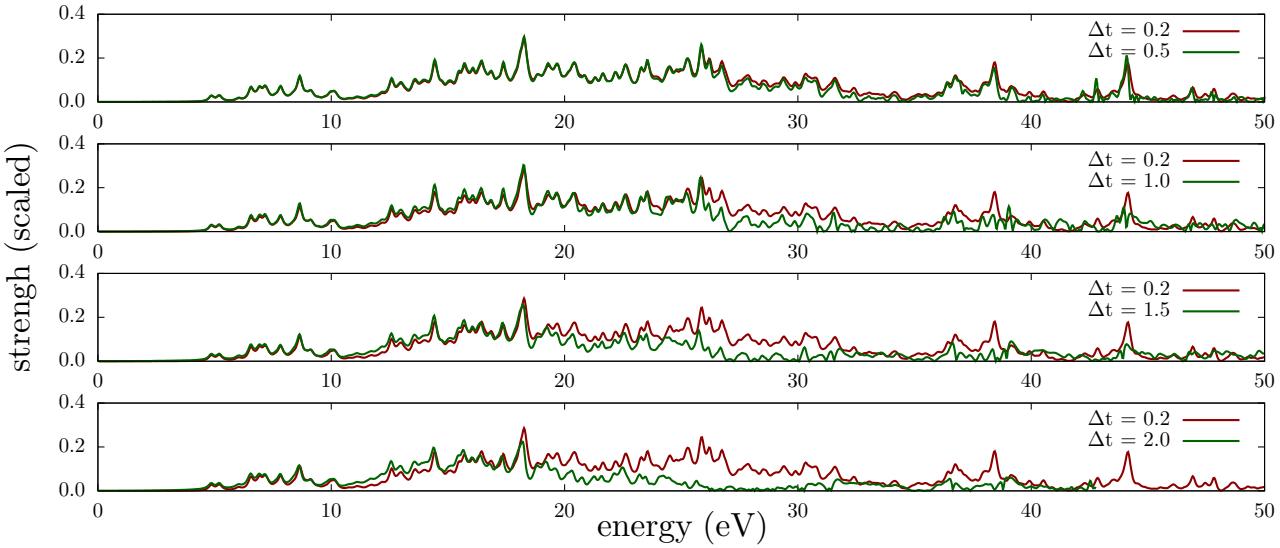

FIG. S18: TDKS spectrum of adenine computed using the EP-PC2 algorithm for various values of Δt. The reference spectrum, computed using $\Delta t = 0.2$ a.u., is shown in red.